Published online 29 July 2022

Nucleic Acids Research, 2022, Vol. 50, No. 15 ***8431–8440***
https://doi.org/10.1093/nar/gkac650

DNA circuits compatible encoder and demultiplexer based on a single biomolecular platform with DNA strands as outputs

Tianci Xie, Yuhan Deng, Jiarui Zhang, Zhen Zhang, Zhe Hu and Tongbo Wu*

School of Pharmacy, Tongji Medical College, Huazhong University of Science and Technology, Wuhan 430030, China

Received February 22, 2022; Revised July 09, 2022; Editorial Decision July 11, 2022; Accepted July 20, 2022

ABSTRACT

A series of multiple logic circuits based on a single biomolecular platform is constructed to perform nonarithmetic and arithmetic functions, including 4-to-2 encoder, 1-to-2 demultiplexer, 1-to-4 demultiplexer, and multi-input OR gate. The encoder to a DNA circuit is the equivalent of a sensory receptor to a reflex arc. They all function to encode information from outside the pathway (DNA circuit or reflex arc) into a form that subsequent pathways can recognize and utilize. Current molecular encoders are based on optical or electrical signals as outputs, while DNA circuits are based on DNA strands as transmission signals. The output of existing encoders cannot be recognized by subsequent DNA circuits. It is the first time the DNA-based encoder with DNA strands as outputs can be truly applied to the DNA circuit, enabling the application of DNA circuits in non-binary biological environments. Another novel feature of the designed system is that the developed nanodevices all have a simple structure, low leakage and low crosstalk, which allows them to implement higher-level encoders and demultiplexers easily. Our work is based on the idea of complex functionality in a simple form, which will also provide a new route for developing advanced molecular logic circuits.

GRAPHICAL ABSTRACT

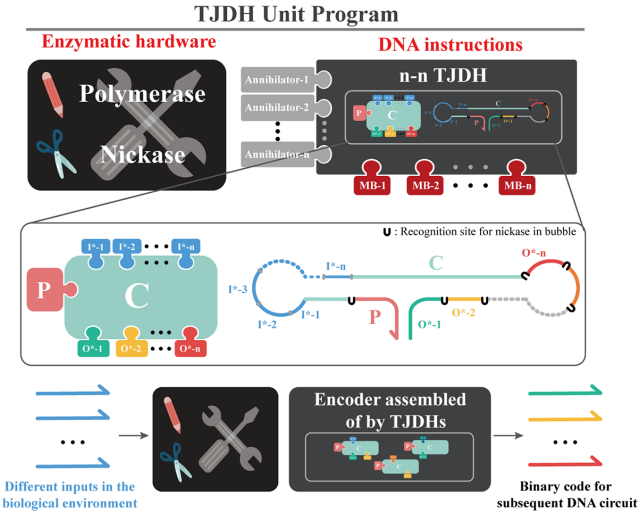

INTRODUCTION

The beauty of life is made possible by ubiquitous computing and information processing at the molecular level. DNA, the most potent information processing medium in living organisms, has been widely used to construct a series of basic logic gates and advanced logic devices due to its good specificity, high flexibility, and easy self-assembly with desirable conformational changes (1–5). As DNA-based devices have much better biocompatibility than silicon-based electronics (6,7), DNA circuits have a bright prospect of being used for environmental monitoring, drug delivery and smart medical diagnostics (8–13).

An encoder is a combinational circuit device that compiles and converts the information into a binary code usable for circuit communication, transmission, and storage. An encoder is often applied as the start of a circuit (14,15). The encoder to a DNA circuit is the equivalent of a sensory receptor to a reflex arc. The sensory receptor receives an adequate stimulus and encodes that stimulus into a nerve impulse that can be recognized and utilized by afferent nerves.

*To whom correspondence should be addressed. Tel: +86 27 83692754; Fax: +86 27 83692754; Email: wutongbo@hust.edu.cn

The encoder recognizes the information (e.g. DNA strands, RNA strands or proteins) in the application scenarios (e.g. environmental monitoring, drug delivery and smart medical diagnostics) (8–13) and encodes this information into a binary code for use in subsequent DNA circuits. The significance of the DNA encoder lies in its ability to convert signals from the biological environment into a binary code that DNA circuits can use for logical operations. To our knowledge, current molecular encoders always use fluorescence or chemiluminescence signals as the output (16–23). As DNA circuits use DNA strands as transmission between components (1–3), the mismatch of their media makes the current molecular encoders unable to provide binary codes for subsequent circuits. Current encoders cannot be utilized to start a DNA circuit. Just as a reflex arc without sensory receptors cannot respond directly to external stimuli, DNA circuits without encoders are extremely limited in their direct application to real-world environments. Thus, the encoder applied in DNA circuits in living organisms' complex and non-binary environments is urgently needed.

The circuit diagram and truth table of the encoder are shown in Supplementary Figure S1 (24). It has a maximum of 2^n input lines and n output lines. It will produce a binary code equivalent to the input. The circuit diagram shows that a 2^n to n encoder requires a composition of $n2^{n-1}$-input OR gates (Supplementary Figure S1A and C) or $n(2^{n-1} - 1)$ 2-input OR gates (Supplementary Figure S1D). Simply stacking encoders with 2-inputs OR gates would significantly increase the number of circuit stages and design difficulty, resulting in considerable leakage and crosstalk. Therefore, the implementation of a multi-input OR gate with a simple design, low crosstalk and signal amplification capability is a way to implement the encoder.

Furthermore, the demultiplexer is a logical related component of the encoder (16). The demultiplexer is a combinational circuit that distributes the single input data to a specific output line. The circuit diagram and truth table of the demultiplexer are shown in Supplementary Figure S2 (24). It has a single input, n selection lines and a maximum of 2^n outputs. The input will be connected to one of these outputs based on the values of selection lines. Since there are n selection lines, there will be 2^n possible combinations of zeros and ones. In simple terms, it assigns signals to the lines you want basing on the selection input.

With multi-input OR gates having multiple input lines and one output line and demultiplexers having one input line and multiple output lines, we want to build a single platform that recognizes *n* inputs and produces *n* outputs (*n*–*n* platform) to implement both of them. An encoder design with DNA strands as outputs is implemented simultaneously. The *n*–*n* platform is relatively easy to implement in DNA logic circuits based on single-stranded gates (SSG) using strand-displacing polymerase (Figure 1A) (25) and the Exponential Amplification Reaction (EXPAR) of nucleic acids using strand-displacing polymerase and nicking enzyme (Figure 1B) (26). However, a large number of single-stranded DNA (ssDNA) with free 3'-OH ends in these systems can generate significant crosstalk and leakage in the presence of polymerase. A schematic illustration of possible sources of background amplification triggered by transient template hybridizations, strand replacement and the subsequent extension by DNA polymerase is shown in Supplementary Figure S3 (27).

Herein, we transform the SSG and EXPAR into a three-way junction-incorporated double hairpin unit (TJDH, Figure 1C) with a simple design to achieve complex functions. In the TJDH reaction system, the three-way junction structure blocked the interaction among the exposed ssDNA in SSG and EXPAR. This advantage could reduce leakage. Moreover, TJDH with palindromic sequences can amplify the output, which ensures that the data distribution function of the TJDH-based demultiplexer is robust even when the signal is degraded. The amplification ability also ensures that the encoder composed of TJDH can generate enough binary code output for subsequent circuits, even in environments with few specific signals (DNA or RNA strands). In addition to non-nucleic acid information (e.g. ions, small molecules, proteins, cells and microorganisms), we can also use aptamers to convert this information into a nucleic acid that can be sensed by TJDH (Supplementary Figure S4) (28). Furthermore, the select output function could be realized with the assistance of annihilators in the demultiplexer. Besides, the TJDH can robustly perform multi-input OR gate functions even in complex secondary structures of input chains.

We have implemented multi-input OR gate, 1-to-2 (1–2) and 1-to-4 (1–4) demultiplexers in this work. More importantly, we have assembled the TJDH into 4-to-2 (4–2) encoders, realizing the first molecular encoder that can be truly applied to DNA circuits and verifying its ability to encode for downstream circuits.

MATERIALS AND METHODS

Materials and apparatus

All oligonucleotides used in this study were synthesized and purified by Tsingke Biotechnology Co., Ltd. (Wuhan, China) and Sangon Biotech Co., Ltd. (Shanghai, China). Vent (exo-) DNA Polymerase (Vent), Nt.BstNBI nicking enzyme (Nt.BstNBI), 10× NEBuffer 3.1 (1 M NaCl, 500 mM Tris–HCl, 100 mM $MgCl_2$, 1 mg/ml BSA, pH 7.9), 10× ThermoPol Reaction Buffer (200 mM Tris–HCl, 100 mM $(NH_4)_2SO_4$, 100 mM KCl, 20 mM $MgSO_4$, 0.1% Triton X-100, pH 8.8) were purchased from New England Biolabs Inc. (Beijing, China). Deoxynucleotides (dNTPs, 2.5 mM) was purchased from Tiangen Biotech Co. Ltd. (Beijing, China). Agarose, 5× TBE Buffer, 4S Red Plus Nucleic Acid Stain, 6× DNA Loading Dye and DNA Marker A (25–500 bp) were purchased from Sangon Biotech Co., Ltd. (Shanghai, China). The concentration of DNA oligonucleotides was measured using a NanoDrop 2000 UV–vis spectrophotometer (Thermo Fisher Scientific, Waltham, MA, USA). The sequences of all oligos are listed in Supplementary Table S1. The secondary structure of TJDHs at 55°C predicted by NUPACK (http://nupack.org/) (29–32) is shown in Supplementary Figure S5.

Fluorescence monitoring

Fluorescence was measured using a LineGene Mini FQD-16A (Bioer Technology Co., Ltd., Hangzhou, China) at 55°C. The fluorescence intensity was recorded every 1 min

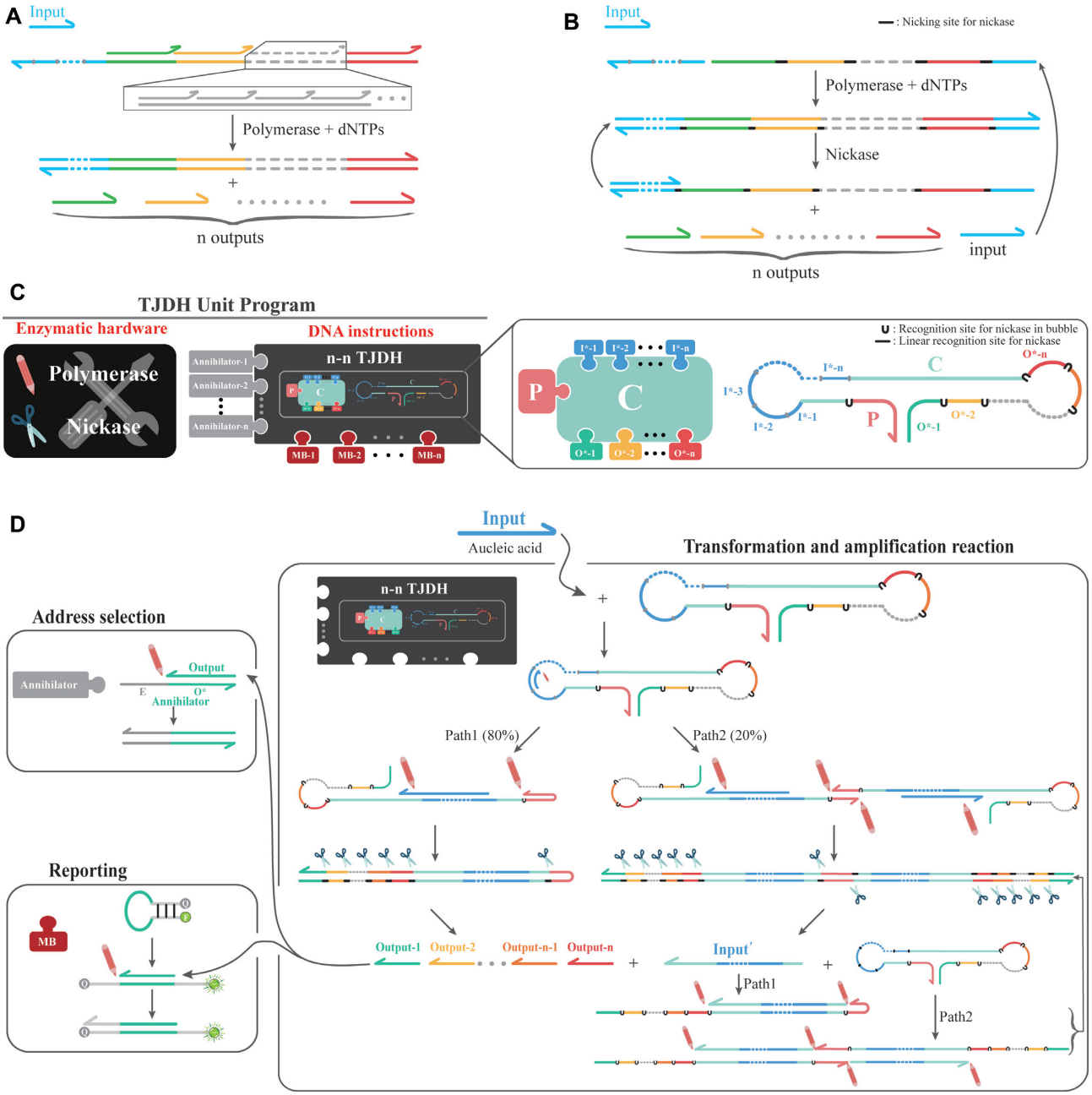

Figure 1. Construction of circuit components in SSG, EXPAR and TJDH. (**A**) *n*–*n* platform (capable of recognizing *n* inputs and generating *n* outputs) in SSG. (**B**) *n*–*n* platform in EXPAR. (**C**) Structure of *n*–*n* TJDH (indicates a TJDH with *n* inputs and *n* outputs) unit program. (**D**) The reactions of the TJDH corresponding to the input, including transformation and amplification reaction, address selection based on annihilator and reporting.

for 2 or 4 h, and the gain levels of the FAM, HEX, ROX and Cy5 channels were 10, 7, 10 and 10, respectively. The excitation and emission wavelengths were set to 470 and 525 nm for the FAM channel, 523 and 564 nm for the HEX channel, 571 and 612 nm for the ROX channel, and 628 and 692 nm for the Cy5 channel.

Agarose gel electrophoresis analysis

Agarose gel electrophoresis was carried out using a 3% agarose gel at 110 V in a 1× TBE buffer. All the samples were prepared in 200 μl PCR tubes and incubated at 55°C for 2 h. Then, 10 μl of sample solution and 2 μl of loading buffer were mixed and added to each well. After the separation in the electrophoresis apparatus (Junyi, Beijing, China), the gels containing DNA were stained using 4S Red Plus and visualized at a wavelength of 590 nm using a Bio-Rad Universal Hood II gel imaging system (Bio-Rad, Shanghai, China).

Preparation for the reaction

TJDH, SSG, And gate, molecular beacon (MB) and reporter were annealed by heating to 95°C for 10 min followed

by cooling to 30°C over 60 min in 1× ThermoPol Reaction Buffer, ensuring that they can form a stable and desirable secondary structure. Reagents for the reaction and the detection of the products were prepared in one vial. Enzymes were added to the vial last and the final total volume of the solution in the vial was kept at 20 μl, and the fluorescence intensity was recorded immediately after enzyme addition.

Optimization of experimental conditions of TJDH

The reaction system consisted of 100 nM 1–2 TJDH, 100 nM MB-1, 100 nM MB-2, 250 μM dNTPs, 0.5× NEBuffer 3.1 and 1× ThermoPol Reaction Buffer. The Control group contained no input-1, and the experimental group contained 100 nM input-1. The concentration of Vent was optimized by keeping the concentration of Nt.BstNBI at 50 U/mL and Vent at 10, 15, 20, 25, 30 U/ml, respectively. The concentration of Nt.BstNBI was optimized by keeping the concentration of Vent at 20 U/mL and Nt.BstNBI at 50, 37.5, 25, 12.5 U/ml, respectively.

Demultiplexer in SSG without considering address selection

The reaction system consisted of 100 nM 1–2 SSG (composed of SSG-1, SSG-2 and SSG-3), 100 nM MB-1, 100 nM MB-2, 250 μM dNTPs, 0.5× NE Buffer 3.1, 1× ThermoPol Reaction Buffer and 20 U/ml Vent. The Control group contained no input-1 and the experimental group contained 100 nM input-1.

EXPAR

The reaction system consisted of 100 nM EXPAR-Template, 100 nM MB-1, 100 nM MB-2, 250 μM dNTPs, 0.5× NEBuffer 3.1, 1× ThermoPol Reaction Buffer, 25 U/ml Nt.BstNBI and 20 U/ml Vent. The Control group contained no input-1 and the experimental group contained 100 nM input-1.

Simulation of operation in signal attenuation condition

The reaction system consisted of 100 nM 1–2 SSG or 100 nM 1–2 TJDH, 100 nM MB-1, 100 nM MB-2, 250 μM dNTPs, 0.5× NEBuffer 3.1, 1× ThermoPol Reaction Buffer and 20 U/ml Vent. For the reaction system with 1–2 TJDH, 25 U/ml Nt.BstNBI was also added. Control group contained no input-1 and the experimental group contained 50 nM (0.5×) input-1.

Detection limits for TJDH

The reaction system consisted of 100 nM 1–1 TJDH-1, 100 nM MB-1, 250 μM dNTPs, 0.5× NEBuffer 3.1, 1× ThermoPol Reaction Buffer, 12.5 U/ml Nt.BstNBI and 10 U/ml Vent. The Control group contained no input-1, and the experimental group contained 10, 25, 50, 100 or 150 nM input-1.

Transformation of the TJDH into a demultiplexer via annihilator

The reaction system consisted of 100 nM 1–2 TJDH or 1–4 TJDH, 100 nM MB-1, 100 nM MB-2, 250 μM dNTPs, 0.5× NEBuffer 3.1, 1× ThermoPol Reaction Buffer, Annihilator for FAM, HEX, ROX or Cy5 channel at various concentrations (0, 100(1×), 200(2×), 300(3×), 400(4×) and 500(5×) nM), 20 U/ml Vent and 25 U/ml Nt.BstNBI. For the reaction system with 1–4 TJDH, 100 nM MB-3, 100 nM MB-4, additional 20 U/ml Vent and 25 U/ml Nt.BstNBI were also added. The Control group contained no input-1, and the experimental group contained 100 nM input-1.

Multi-input OR gates

The reaction system consisted of 100 nM 3–1 TJDH or 100 nM Multi-input OR gates in SSG (composed of SSG-4 and SSG-5), 100 nM MB-1, 250 μM dNTPs, 0.5 × NEBuffer 3.1, 1× ThermoPol Reaction Buffer and 10 U/ml Vent. For the reaction system with 3-1 TJDH, 12.5 U/ml Nt.BstNBI was also added. The Control group contained no inputs, and the experimental group contained inputs (I-1, I-2 and I-3) whose concentration was 100 nM each.

4–2 Encoder

The reaction system consisted of 100 nM 1–1 TJDH-1, 100 nM 1–1 TJDH-2, 100 nM 1–2 TJDH, 100 nM Input (I-0, I-1, I-4 or I-5), 100 nM MB-1, 100 nM MB-2, 250 μM dNTPs, 0.5× NEBuffer 3.1, 1× ThermoPol Reaction Buffer, 20 U/ml Vent and 25 U/ml Nt.BstNBI.

Encoder in the DNA circuit

The reaction system consisted of 100 nM 1-1 TJDH-1, 100 nM 1-1 TJDH-2, 100 nM 1–2 TJDH, 100 nM Input (I-0, I-1, I-2 or I-3), 100 nM And gates (composed of And-1, And-2 and And-3), 100 nM reporter (composed of Reporter-1 and Reporter-2), 250 μM dNTPs, 0.5 × NEBuffer 3.1, 1× ThermoPol Reaction Buffer, 20 U/ml Vent and 25 U/ml Nt.BstNBI.

RESULTS AND DISCUSSION

Principle of TJDH mediated amplification reaction

TJDH is the structural basis of our experiments. The structure and reaction program of the TJDH unit are shown in Figure 1C. In TJDH, I* is the region complementary to the input (I), O* is complementary to the output (O), P is the palindromic sequence, and C is the complementary zone. I* can be divided into n segments, corresponding to n inputs. O* can also be divided into n segments, corresponding to n outputs. Here, the input is defined as the DNA strands that could react with the TJDH template to trigger the polymerase elongation. The output is defined as the DNA strands that could react with the downstream molecular beacons. The length requirements of input and output sequences are discussed in Supplementary Discussion S1. An '*n*–*n*' TJDH means that the TJDH could deal with the input number up to *n* (the former), and the output number is *n* (the latter). In the initial state, the template forms a three-way junction structure with two hairpins. There are no free bare ssDNA chains, which significantly reduces the background signal. As shown in Figure 1D, after I hybridizes with TJDH, the three-way junction structure will be destroyed by the involvement of polymerase.

Then the TJDH/I duplexes are self-hybridized (Path1, 80%) or inter-hybridized (Path2, 20%) by the exposed P (Supplementary Figure S6, Supplementary Figure S7 and Supplementary Discussion S2). Then, with the reaction of DNA polymerase, TJDH/I forms a complete long hairpin (Path1) or long double-stranded DNA (dsDNA) (Path2), and I is displaced to react with another TJDH. With the Vent polymerase and Nt.BstNBI (the enzymes used in the reaction system are discussed in Supplementary Discussion S3), the Input' (I') and O could be produced. I' consists of the sequence of I and two regions complementary to C. I' could also hybridize with a new TJDH to trigger the reaction. Thus, one input becomes two inputs after one reaction round, resulting in an amplification reaction. The palindromic sequence provided two paths for the reaction, and we named it dual-path amplification (DP-A). A molecular beacon (MB) reacts with outputs and provides fluorescent signals. MB characterizes the output yield and mimics downstream reactions in the DNA circuit. The reaction of the TJDH platform and its products were characterized using agarose gel electrophoresis (Supplementary Figure S7 and Supplementary Discussion S2). Annihilator could compete with MB to block the output to realize the address selection function.

Optimization of experimental conditions and comparison with SSG and EXPAR

We start with 1–2 TJDH. The detailed reaction process of 1–2 TJDH is shown in Supplementary Figure S8. In theory, the amplification efficiency of DP-A mainly relies on the synergy of polymerase and nickase. The amounts of Vent polymerase and Nt.BstNBI nickase were optimized by changing one experimental condition and keeping the consistency of the other parameters. The average signal-to-noise ratio (Avg (F/F_0)) was used to evaluate the results. F and F_0 are the fluorescence intensities of the individual channel at 90 min with or without the input, respectively. The fluorescence changes and the average signal-to-noise ratio at different enzyme concentrations are shown in Supplementary Figure S9 and discussed in Supplementary Discussion S4. Avg(F/F_0) reached a maximum when the concentrations of Vent and Nt.BstNBI were 20 U/ml and 25 U/ml, respectively, so our subsequent experiments were performed based on this condition. Figure 2 shows that the Avg(F/F_0) of TJDH at the optimum enzyme concentration is much higher than that of SSG and EXPAR, which indicates that our modified structure has minimal leakage and crosstalk. This high robustness creates the possibility of subsequent encoder assembly. We analyzed the reasons for the extremely high background signal possessed by the SSG and EXPAR. Firstly, SSG and EXPAR have many single chains and 3′-OH ends. Coupled with sufficient polymerase, any small portion of transient template hybridizations will result in a significant background signal (Supplementary Figure S3A–C). Secondly, the free 3′-OH of the output strands in the SSG may bind directly to the molecular beacon or downstream circuit to undergo a strand replacement in the absence of the input and directly react with the assistance of polymerase (Supplementary Figure S3D).

In addition, to demonstrate the general applicability of TJDH to the number of outputs, we obtained 1–4 TJDH (Supplementary Figure S10A) by simply adding two more cleavage sites, extending the length of the template strand, and doubling the enzyme concentration. The result in Supplementary Figure S10B shows high robustness comparable to 1–2 TJDH, which creates the possibility of implementation of multithreading demultiplexers and encoders.

Simulation of operation in signal attenuation condition

In addition to its high robustness, another feature of the TJDH compared to other DNA logic gates is its nucleic acid amplification capability. In addition to background signals and crosstalk, attenuation of the target signal is another great challenge for DNA circuits. The TJDH's amplification capability enables it to perform data distribution robustly even in circuits with attenuated signals and generate more transmitted signals for subsequent circuits. It also enables the encoder to generate enough binary code output for subsequent circuits, even in biological environments with low specific signals (inputs). We simulated the signal attenuation phenomenon in the circuit by scaling down the input concentration from 1× (100 nM) to 0.5× (50 nM). Because the crosstalk and leakage of EXPAR were too high, we only compared the resistance to signal attenuation of the TJDH and SSG. When the input was reduced to half, the signal of TJDH (blue and red solid lines in Figure 2E) was significantly higher than the half signal of the 1 × input (blue and red solid lines in Figure 2A), maintaining a high signal-to-noise ratio. In contrast, When the input was reduced to half, the signal of SSG (blue and red solid lines in Figure 2F) reduced to half of the signal of the 1× input (blue and red solid lines in Figure 2B), and the signal-to-noise ratio was poor.

For subsequent circuit-related experiments, we make these rules. For the input, when the concentration is >10 nM, it is defined as the 1 state, while the input with lower (to 0) concentrations is the 0 state. For the output, after reacting with the molecular beacons, if the fluorescence intensity is >3000, it is the 1 state. If the fluorescence intensity is smaller than 3000, it is the 0 state.

We also evaluated the detection limit of 1–1 TJDH-1 to validate the sensitivity of the TJDH platform. In our DP-A, the signal is obtained only when enough input is accumulated. We can calculate the average and standard error of the initial background fluorescence intensity in one fluorescence response curve, find the fluorescence intensity value that is ten times of the background standard error larger than the background average, and define the time of this value in the fluorescence response curve as the rising time. By taking the signal rising time as the analysis criterion, it is easier to draw the standard curve and quantify the concentration of input (Supplementary Figure S11). The limit of detection (LOD) was calculated to be 0.67 nM ($3\sigma/K$). If the threshold of the fluorescent intensity is set at 3000 a.u. with our instrument, the minimal concentration of the input should be around 10 nM. In contrast, other molecule encoders require input concentrations of 100 nM or more (16–23), as none of them has amplification capabilities. Our platform shows better sensitivity than current encoders. How-

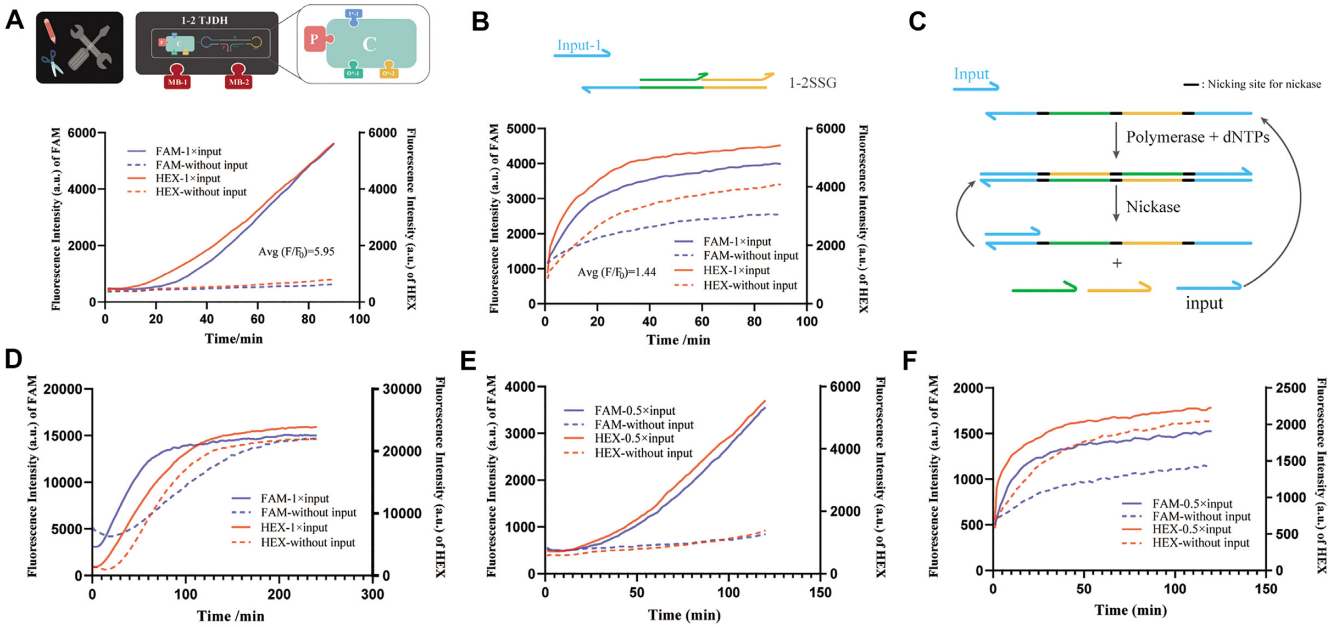

Figure 2. Comparison of performance between circuit components in TJDH, SSG and EXPAR. (**A**) The fluorescence changes and the average signal-to-noise ratio of 1–2 TJDH at the optimum enzyme concentrations. (**B**) The fluorescence changes and the average signal-to-noise ratio of 1–2 SSG at the optimum enzyme concentrations. (**C**) Detailed reaction process of 1–2 EXPAR. (**D**) the fluorescence changes of 1–2 EXPAR at the optimum enzyme concentrations. (E, F) Simulation of operation in signal attenuation (0.5 × input). (**E**) 1–2 TJDH. (**F**) 1–2 SSG.

ever, the detection limit of DP-A is not as good as that of the conventional EXPAR reaction (26,27), which we speculate is due to the long chain of TJDH and the complex reaction procedure, which also limits its sensing of much lower concentrations of biomolecules.

Transformation of the TJDH into a demultiplexer via annihilator

The outputs should be selectable in an ideal demultiplexer to achieve the address selection function. So, we introduced annihilators to eradicate the unwanted outputs. As shown in Figure 1D, the annihilator consists of an O* region complementary to the output and an extended E region with an arbitrary sequence. When the annihilator presents, it competes with the downstream circuit progenitor to react with the output. The annihilator/output duplex could not react with the MB to produce the signal. The annihilator suppressed the signal as low as the background when the annihilator concentration was 5 times as much as the MB (Supplementary Figure S12). Figure 3 shows the graph of fluorescence results with a truth table for 1–2 demultiplexer based on TJDH. Owning to the high robustness of TJDH, the fluorescence change when $D_0 = 0$ is the same as when there are no inputs nor annihilators, so the fluorescence change graph only shows the situation when $D_0 = 1$. The results show that the annihilator has good specificity and does not affect the signal of other channels. The truth table and result plot of the 1–4 demultiplexers are shown in Supplementary Figure S13 and Figure S14.

The robustness of its core structure, TJDH, ensures low crosstalk and low leakage of the demultiplexer. Furthermore, the diversity of its output numbers allows the 1-to-n demultiplexer to be implemented with a simple modification of the template sequence.

Multi-input OR gates

TJDH can also act as a multi-input OR gate. We compare the performance of the TJDH-based multi-input OR gate (Figure 4A) with the SSG-based multi-input OR gate (Figure 4B). Figure 4C and D show the plots of fluorescence detection results for these two gates in the presence of input-1, input-2 or input-3, respectively. With the TJDH-based multi-input OR gate, all three inputs can eventually produce enough output to hybridize with all molecular beacons downstream, resulting in almost the same maximum fluorescence value (Figure 4C). However, with the SSG-based multi-input OR gate, the fluorescence signal cannot reach its maximum in the presence of input-3, indicating that the expected amount of output cannot be produced, and a severe signal attenuation occurs. We speculate that the secondary structure of inputs may hinder their reaction with TJDH and SSG (Figure 4E). TJDH benefits from amplifying with less input and ensures sufficient outputs. In comparison, SSG does not have this ability and is left to decay the signal. In addition, the low background of TJDH still showed its high robustness.

Encoder and its application in circuits

Last but not least, the TJDH was assembled into a 4–2 encoder (Figure 5A). Different signal chains in the environment correspond to different I* regions of different TJDH platforms, thus generating different binary output chains. For the 4–2 encoder in Figure 5A, when input-4 is present in the environment, input-1 will bind to 1-1 TJDH-1 and

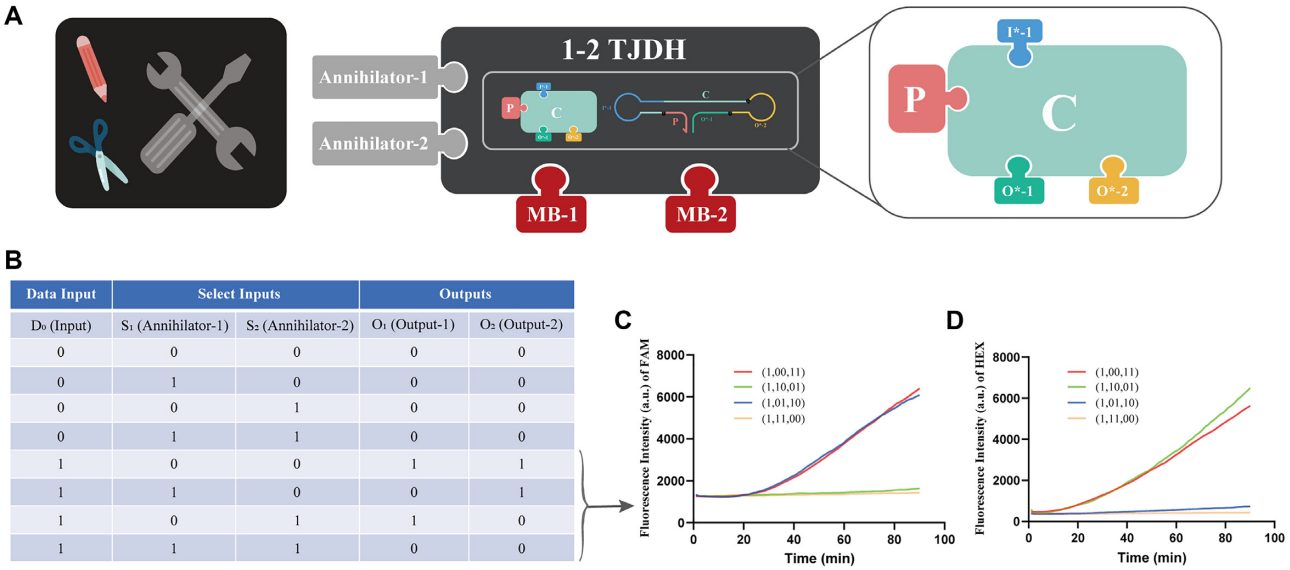

Data Input	Select Inputs		Outputs	
D_0 (Input)	S_1 (Annihilator-1)	S_2 (Annihilator-2)	O_1 (Output-1)	O_2 (Output-2)
0	0	0	0	0
0	1	0	0	0
0	0	1	0	0
0	1	1	0	0
1	0	0	1	1
1	1	0	0	1
1	0	1	1	0
1	1	1	0	0

Figure 3. 1–2 demultiplexer based on 1–2 TJDH and annihilators. (**A**) Schematic diagram of the program that implements the 1–2 demultiplexer based on 1–2 TJDH. (**B**) The corresponding truth table of the 1–2 demultiplexer. (**C**) Fluorescence responses of the FAM channel of 1–2 demultiplexer under different annihilators. (1,00,11) represents $D_0 = 1$, $S_1 = 0$, $S_2 = 0$, $O_1 = 1$, $O_2 = 1$, and so on. (**D**) Fluorescence responses of the HEX channel of 1–2 demultiplexer under different annihilators.

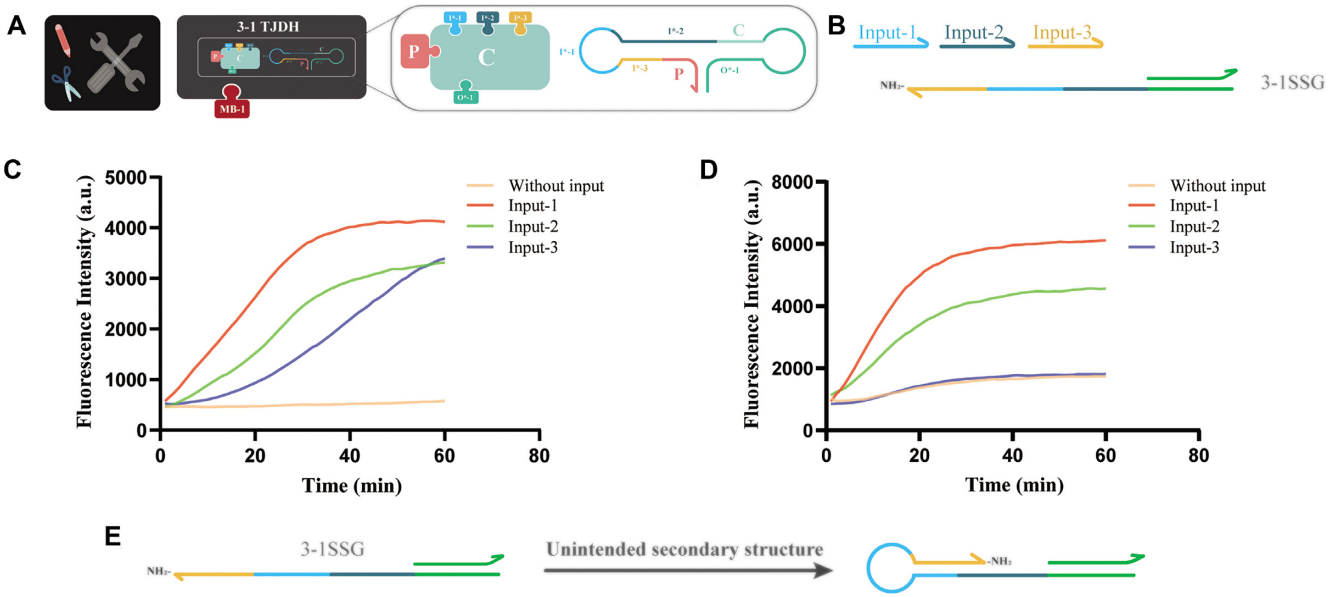

Figure 4. Multi-input OR gates. (**A**) Schematic diagram of the program that implements the TJDH based 3-input OR gate. (**B**) Schematic diagram of the program that implements the SSG based 3-input OR gate. (**C**) Fluorescence responses of TJDH based 3-input OR gate under different inputs. (**D**) Fluorescence responses of SSG based 3-input OR gate under different inputs. (**E**) The unintended secondary structure formed by the 3–1 SSG prevents the input-2 and input-3 from binding to the 3–1 SSG.

produce output-1 via the DP-A. When input-5 is present, it will bind to 1–1 TJDH-2 and produce output-2. When Input-1 is present, it will bind to 1–2 TJDH and produce output-1 and output-2. When input-0 is present, no outputs will be produced because there is no TJDH corresponding to it. In this way, the complex biological signals could be converted into the corresponding binary code. The truth table of the 4–2 encoder is shown in Figure 5B. The fluorescence curve (Figure 5C and D) shows that TJDH continues to demonstrate its high robustness. Characterization of the reaction process of the 4–2 encoder using gel electrophoresis is shown in Supplementary Figure S15. To our knowledge, this is the platform with the highest signal-to-noise ratio for performing such complex functions in DNA circuits and is the first encoder capable of truly programming and converting signals for DNA circuits. We wired the 4-2 encoder to the beginning of a DNA circuit to further verify the encoder's ability to encode for subsequent circuits. The

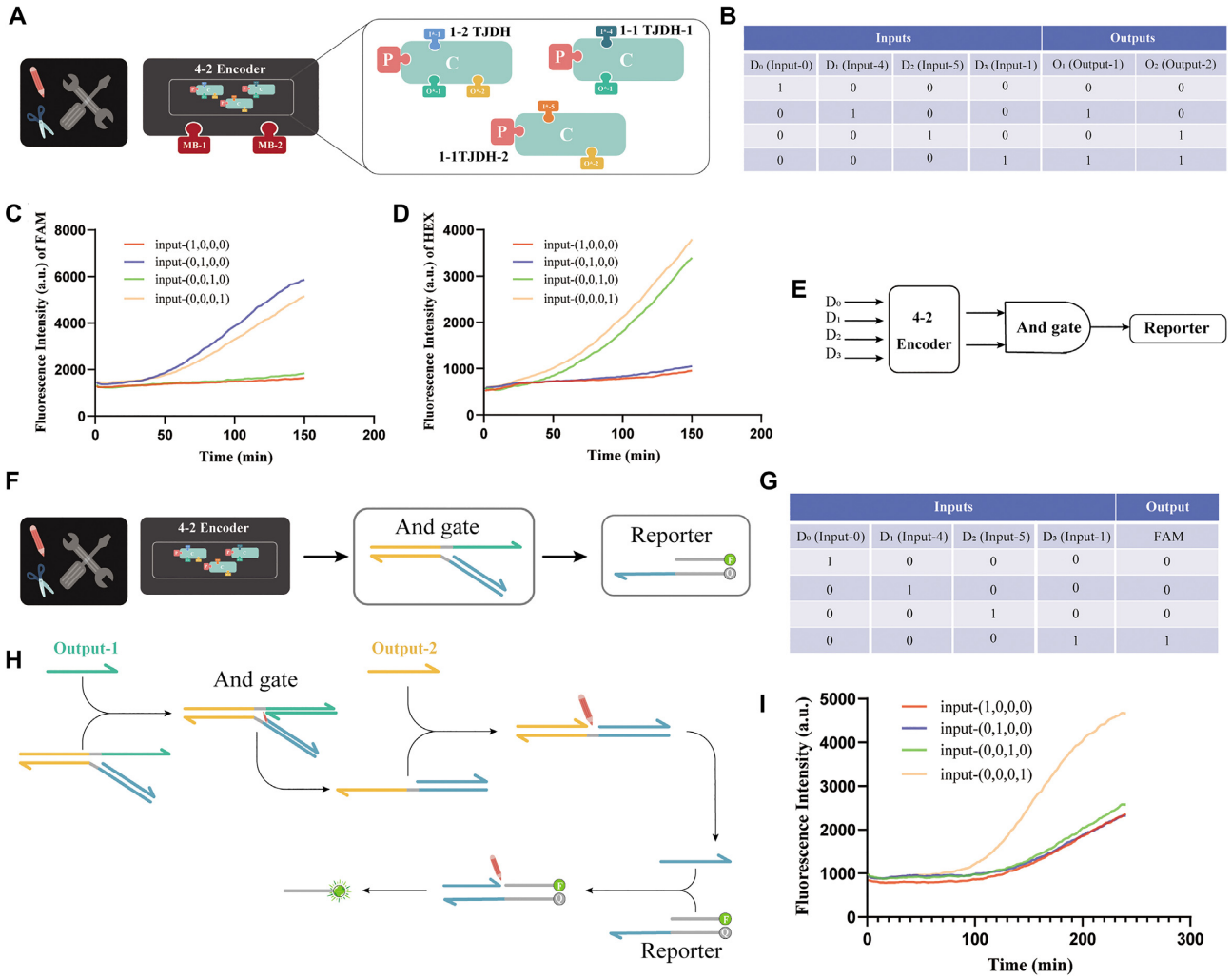

Inputs				Outputs	
D_0 (Input-0)	D_1 (Input-4)	D_2 (Input-5)	D_3 (Input-1)	O_1 (Output-1)	O_2 (Output-2)
1	0	0	0	0	0
0	1	0	0	1	0
0	0	1	0	0	1
0	0	0	1	1	1

Inputs				Output
D_0 (Input-0)	D_1 (Input-4)	D_2 (Input-5)	D_3 (Input-1)	FAM
1	0	0	0	0
0	1	0	0	0
0	0	1	0	0
0	0	0	1	1

Figure 5. Construction of the 4-2 encoder from TJDHs. (**A**) The schematic illustration and (**B**) truth table of the TJDH-based 4-2 encoder. (**C**) Fluorescence spectra of the FAM channel of the TJDH-based 4-2 encoder under different logic operations. (**D**) Fluorescence spectra of the HEX channel of the TJDH-based 4-2 encoder under different logic operations. (**E**) The logic circuit, (**F**) schematic illustration and (**G**) truth table of the three-stage circuit starting with the TJDH-based 4-2 encoder. (**H**) The schematic of And gate and Reporter. (**I**) Fluorescence spectra of the three-stage circuit under different logic operations.

logic circuit, schematic illustration and truth table of this three-stage circuit are shown in Figure 5E, F and G, respectively. The schematic of the subsequent circuit is shown in Figure 5H. Figure 5I shows that the signal and background are still clearly distinguishable even when the encoder is placed in a circuit with three levels. Thus, the TJDH-based encoder could be used in a real circuit, which is a breakthrough for molecular encoders. It is the first connection between molecular encoders and DNA circuits. Moreover, the fluorescence curves of Figure 5I show similar trends when the inputs are (1,0,0,0), (0,1,0,0), and (0,0,1,0), and combined with previous reports in the literature on the results of logic gates involving polymerase in multilevel circuits (2), we speculate that the background signal comes more from the downstream circuit than from the encoder itself, the speculation was verified using agarose gel electrophoresis (Supplementary Figure S15 and Supplementary Discussion S5).

CONCLUSION

Current DNA circuits are mostly stacked with AND gates or OR gates to form complex components. As the functions become more complex and the circuit size becomes larger, crosstalk and leakage will inevitably increase dramatically, one of the major hindrances to the development of current DNA circuits (1–3). Although complex circuit elements such as encoders, decoders, multiplexers and demultiplexers have been implemented, they all resorted to complex structure or non-biological materials such as nanogold and graphene. More importantly, current molecular encoder only completes the logical function alone, with optical signals as outputs. Therefore, they cannot be connected to the DNA circuit, defeating the original purpose of designing encoders for the circuit (16–23).

In this work, we designed a three-way junction-incorporated double hairpin unit, TJDH. TJDH platform is robust with low crosstalk and low leakage. The sys-

tem has no introduction of non-biological materials and exhibits extremely high robustness. Furthermore, its amplification capability can easily cope with signal attenuation in the circuit or too small concentrations of recognized chains in the biological environment. TJDH could be used as a multi-input OR gate with lower leakage and lower input sequence requirements than the SSG-based multi-input OR gate. The TJDH can also be turned into a demultiplexer when annihilators are introduced. Based on TJDH, we implemented the first molecular encoders in a single platform with DNA strands as outputs. The encoder has proven to be truly applicable in DNA circuits. Our design concept of 'complex functions in a single simple platform' sets the stage for developing more complex DNA circuits in the future. However, this work has some limitations, such as the detection limit is not yet sufficient for lower concentrations of nucleic acids. For other biomolecular information, we can only use aptamers to convert them into nucleic acids, and the aptamers are limited. So, this work cannot sense those biomolecules that do not have aptamers. This work is only the first small step towards an encoder that can be truly used in DNA circuits. We are confident that in the near future, more powerful molecular encoders will be realized that will significantly expand the range of DNA applications for DNA circuits.

DATA AVAILABILITY

All data supporting the findings of this study are available within the Article and its Supplementary Information, or from the corresponding author upon reasonable request.

SUPPLEMENTARY DATA

Supplementary Data are available at NAR Online.

ACKNOWLEDGEMENTS

Author contributions: T.X. and T.W. conceived the study. T.W. led the project. T.X. designed the experiment, analyzed the experiment data and performed most experiment. Y.D. J.Z., Z.Z. and Z.H. participated in the experiments and provided useful discussion. T.X. drafted the paper and T.W. revised the paper.

FUNDING

National Natural Science Foundation of China [82172372, 21904045]; Fundamental Research Funds for the Central Universities [2021yjsCXCY127, 2019kfyXJJS169]; Training Program of Innovation and Entrepreneurship for Undergraduates of Hubei Province [S202110487367]. Funding for open access charge: National Natural Science Foundation of China.

Conflict of interest statement. None declared.

REFERENCES

1. Qian,L. and Winfree,E. (2011) Scaling up digital circuit computation with DNA strand displacement cascades. *Science*, **332**, 1196–1201.
2. Su,H., Xu,J., Wang,Q., Wang,F. and Zhou,X. (2019) High-efficiency and integrable DNA arithmetic and logic system based on strand displacement synthesis. *Nat. Commun.*, **10**, 5390.
3. Song,T., Eshra,A., Shah,S., Bui,H., Fu,D., Yang,M., Mokhtar,R. and Reif,J. (2019) Fast and compact DNA logic circuits based on single-stranded gates using strand-displacing polymerase. *Nat. Nanotechnol.*, **14**, 1075–1081.
4. Garg,S., Shah,S., Bui,H., Song,T., Mokhtar,R. and Reif,J. (2018) Renewable time-responsive DNA circuits. *Small*, **14**, e1801470.
5. Xiong,X., Xiao,M., Lai,W., Li,L., Fan,C. and Pei,H. (2021) Optochemical control of DNA-Switching circuits for logic and probabilistic computation. *Angew. Chem. Int. Ed. Engl.*, **60**, 3397–3401.
6. Fu,T., Lyu,Y., Liu,H., Peng,R., Zhang,X., Ye,M. and Tan,W. (2018) DNA-Based dynamic reaction networks. *Trends Biochem. Sci.*, **43**, 547–560.
7. Chen,Y.J., Groves,B., Muscat,R.A. and Seelig,G. (2015) DNA nanotechnology from the test tube to the cell. *Nat. Nanotechnol.*, **10**, 748–760.
8. Lopez,R., Wang,R. and Seelig,G. (2018) A molecular multi-gene classifier for disease diagnostics. *Nat. Chem.*, **10**, 746–754.
9. Zhang,C., Zhao,Y., Xu,X., Xu,R., Li,H., Teng,X., Du,Y., Miao,Y., Lin,H.C. and Han,D. (2020) Cancer diagnosis with DNA molecular computation. *Nat. Nanotechnol.*, **15**, 709–715.
10. Tregubov,A.A., Nikitin,P.I. and Nikitin,M.P. (2018) Advanced smart nanomaterials with integrated logic-gating and biocomputing: dawn of theranostic nanorobots. *Chem. Rev.*, **118**, 10294–10348.
11. Lin,X., Liu,Y., Deng,J., Lyu,Y., Qian,P., Li,Y. and Wang,S. (2018) Multiple advanced logic gates made of DNA-Ag nanocluster and the application for intelligent detection of pathogenic bacterial genes. *Chem. Sci.*, **9**, 1774–1781.
12. Hu,Q., Li,H., Wang,L., Gu,H. and Fan,C. (2019) DNA nanotechnology-enabled drug delivery systems. *Chem. Rev.*, **119**, 6459–6506.
13. Jiang,S.X., Ge,Z.L., Mou,S., Yan,H. and Fan,C.H. (2021) Designer DNA nanostructures for therapeutics. *Chem.*, **7**, 1156–1179.
14. Badrinarayanan,V., Kendall,A. and Cipolla,R. (2017) SegNet: a deep convolutional encoder-decoder architecture for image segmentation. *IEEE Trans. Pattern Anal. Mach. Intell.*, **39**, 2481–2495.
15. Song,J.K., Zhang,H.W., Li,X.P., Gao,L.L., Wang,M. and Hong,R.C. (2018) Self-Supervised video hashing with hierarchical binary auto-encoder. *IEEE Trans. Image Process.*, **27**, 3210–3221.
16. Kang,D., White,R.J., Xia,F., Zuo,X., Vallée-Bélisle,A. and Plaxco,K.W. (2012) DNA biomolecular-electronic encoder and decoder devices constructed by multiplex biosensors. *NPG Asia Materials*, **4**, e1.
17. He,Y., Chen,Y., Li,C. and Cui,H. (2014) Molecular encoder-decoder based on an assembly of graphene oxide with dye-labelled DNA. *Chem. Commun. (Camb.)*, **50**, 7994–7997.
18. Liu,S., Li,M., Yu,X., Li,C.Z. and Liu,H. (2015) Biomacromolecular logic gate, encoder/decoder and keypad lock based on DNA damage with electrochemiluminescence and electrochemical signals as outputs. *Chem. Commun. (Camb.)*, **51**, 13185–13188.
19. Li,H., Liu,Y., Dong,S. and Wang,E. (2015) DNA-based advanced logic circuits for nonarithmetic information processing. *NPG Asia Materials*, **7**, e166.
20. Wu,C., Zhou,C., Wang,E. and Dong,S. (2016) A label-free and enzyme-free system for operating various logic devices using poly(thymine)-templated cunps and SYBR green i as signal transducers. *Nanoscale*, **8**, 14243–14249.
21. Fan,D., Zhu,J., Liu,Y., Wang,E. and Dong,S. (2016) Label-free and enzyme-free platform for the construction of advanced DNA logic devices based on the assembly of graphene oxide and DNA-templated AgNCs. *Nanoscale*, **8**, 3834–3840.
22. Zhang,S., Wang,K., Huang,C., Li,Z., Sun,T. and Han,D.M. (2016) An enzyme-free and resettable platform for the construction of advanced molecular logic devices based on magnetic beads and DNA. *Nanoscale*, **8**, 15681–15688.
23. Gao,R.R., Yao,T.M., Lv,X.Y., Zhu,Y.Y., Zhang,Y.W. and Shi,S. (2017) Integration of G-quadruplex and DNA-templated ag NCs for nonarithmetic information processing. *Chem. Sci.*, **8**, 4211–4222.
24. Collier,M., Bebova,S. and Wei,W. (2014) In: *Digital Circuit Design: Principles and Practice*. CreateSpace Independent Publishing Platform, Charleston, South Carolina, USA.

25. Shah,S., Wee,J., Song,T., Ceze,L., Strauss,K., Chen,Y.J. and Reif,J. (2020) Using strand displacing polymerase to program chemical reaction networks. *J. Am. Chem. Soc.*, **142**, 9587–9593.
26. Reid,M.S., Le,X.C. and Zhang,H. (2018) Exponential isothermal amplification of nucleic acids and assays for proteins, cells, small molecules, and enzyme activities: an EXPAR example. *Angew. Chem. Int. Ed Engl.*, **57**, 11856–11866.
27. Reid,M.S., Paliwoda,R.E., Zhang,H.Q. and Le,X.C. (2018) Reduction of background generated from template-template hybridizations in the exponential amplification reaction. *Anal. Chem.*, **90**, 11033–11039.
28. Wu,N., Zhang,X.Y., Xia,J., Li,X., Yang,T. and Wang,J.H. (2021) Ratiometric 3D DNA machine combined with machine learning algorithm for ultrasensitive and high-precision screening of early urinary diseases. *ACS Nano*, **15**, 19522–19534.
29. Dirks,R.M. and Pierce,N.A. (2004) An algorithm for computing nucleic acid base-pairing probabilities including pseudoknots. *J. Comput. Chem.*, **25**, 1295–1304.
30. Dirks,R.M., Bois,J.S., Schaeffer,J.M., Winfree,E. and Pierce,N.A. (2007) Thermodynamic analysis of interacting nucleic acid strands. *SIAM Rev.*, **49**, 65–88.
31. Zadeh,J.N., Steenberg,C.D., Bois,J.S., Wolfe,B.R., Pierce,M.B., Khan,A.R., Dirks,R.M. and Pierce,N.A. (2011) NUPACK: analysis and design of nucleic acid systems. *J. Comput. Chem.*, **32**, 170–173.
32. Fornace,M.E., Porubsky,N.J. and Pierce,N.A. (2020) A unified dynamic programming framework for the analysis of interacting nucleic acid strands: enhanced models, scalability, and speed. *ACS Synth. Biol.*, **9**, 2665–2678.